Journal of the Korean Ceramic Society
Vol. 53, No. 1, pp. 56~62, 2016.

http://dx.doi.org/10.4191/kcers.2016.53.1.56

Novel Bi_2S_3/TiO_2 Heterogeneous Catalyst: Photocatalytic Mechanism for Decolorization of Texbrite Dye and Evaluation of Oxygen Species

Lei Zhu and Won-Chun Oh†

Department of Advanced Materials Science & Engineering, Hanseo University, Seosan 31962, Korea

(Received August 21, 2015; Revised October 16, 2015; Accepted October 27, 2015)

ABSTRACT

A heterogeneous Bi_2S_3/TiO_2 composite catalyst was synthesized via a green ultrasonic-assisted method and characterized by XRD, SEM, EDX, TEM analysis. The results clearly show that the TiO_2 particles were homogenously coated with Bi_2S_3 particles, indicating that Bi_2S_3 particle agglomeration was effectively inhibited after the introduction of anatase TiO_2. The Texbrite BA-L (TBA) degradation rate constant for Bi_2S_3/TiO_2 composites reached 8.27×10^{-3} min^{-1} under visible light, much higher than the corresponding value of 1.04×10^{-3} min^{-1} for TiO_2. The quantities of generated hydroxyl radicals can be analyzed by DPCI degradation, which shows that under visible light irradiation, more electron–hole pairs can be generated. Finally, the possible mechanism for the generation of reactive oxygen species under visible-light irradiation was proposed as well. Our result shows the significant potential of Bi_2S_3-semiconductor-based TiO_2 hybrid materials as catalysts under visible light for the degradation of industry dye effluent substances.

Key words : Heterogeneous, Sonochemical, Visible light, Bi_2S_3, DPCO

1. Introduction

This diminishing health of the environment demands the introduction of new ways to prevent serious environmental issues caused by organic dyes. However, the actual threat to the environment by these dyes occurs during their extraction phase. It is well recognized that these dyes and their products (such as amines) are highly toxic in nature.[1)] The waste from these dyes can cause damage to the skin, eyes, and respiratory tract system, and can lead to chronic health defects.[2)] Texbrite MST-L is used commercially for padding and filling or for dyeing textile products such as polyester and cotton fabrics. However, such dyes are directly or indirectly hazardous to the environment and to human life. To address this, several schemes have been introduced related to degradation and purification technology to heal the environment. These techniques, including coagulation, flocculation, and adsorption, have been used to decolorize textile effluents. However, a number of limitations reduce the commercial usage of these methods, such as sludge generation, absorbency, and membrane fouling.[3)]

TiO_2 has attracted much attention over the last few decades, not only for its effectiveness when used with photoelectric conversion and photocatalysis but also for its low cost, simple production processes, good photochemical and biological stability, and innocuity with regard to the environment and humans.[4,5)] However, TiO_2 has a wide energy bandgap of 3.2 eV and can thus be excited only by ultraviolet light, which is only 4 - 6% of the solar spectrum. Therefore, TiO_2 nanoparticles cannot efficiently utilize the solar energy. In addition, the high recombining probability of electrons and holes photogenerated in TiO_2 would decrease its photocatalytic activity. All of these drawbacks limit its application, especially in large-scale industries. To solve the above problems, many methods have been applied to extend the light absorption of TiO_2 into the visible region and increase its photocatalytic activity. Various semiconductors, including CdS,[6)] PbS,[7)] CdSe,[8,9)] have been investigated to sensitize TiO_2 as a visible light absorber. Among these semiconductors, Bi_2S_3 has shown promise in thermoelectric and optoelectronic applications as well as biological and chemical sensors. With a direct bandgap of 1.3 eV, bismuth sulfide (Bi_2S_3) exhibits promising applications in photovoltaic converters and thermoelectric cooling technologies based on the Peltier effect.[10)] Yu *et al.*[11)] reported by means of a two-step method that TiO_2 nanoparticles also could be grown on the {310} facet of pre-prepared Bi_2S_3 nanorods to form heterostructures but with interfacial defects. The charge transfer in heterostructures with different interfaces was evaluated by the photodegradation of methyl orange under visible-light irradiation. Bessekhouad *et al.*[12)] published related research. Nevertheless, one issue related to their study was that the proportion of Bi_2S_3 in Bi_2S_3/TiO_2 heterojunction increased from 10 wt.% to 50 wt.%, with an increase of 20 wt.% each time. Therefore, it remains important to study in detail the

†Corresponding author : Won-Chun Oh
E-mail : wc_oh@hanseo.ac.kr
Tel : +82-41-660-1337 Fax : +82-41-688-3352

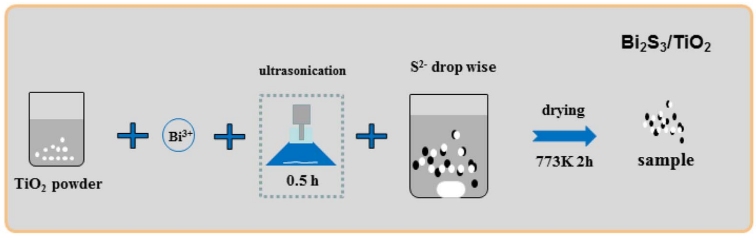

Fig. 1. Schematic illustration of the deposition of Bi_2S_3 nanoparticles onto TiO_2.

influence of different preparation methods for Bi_2S_3/TiO_2 heterojunctions on their photocatalytic activity.

A sonochemical method is a facile route which is operated under ambient conditions. Ultrasonic irradiation causes cavitation in a liquid medium, where the formation, growth and implosive collapse of bubbles occurs. The collapse of bubbles with short lifetimes produces intense local heating and high pressure levels. These localized hot spots can generate temperatures of approximately 5000°C and pressure levels which exceed 1800 kPa, making the spots appropriate for many chemical reactions.[13,14] Recently, Wang *et al.*[15] successfully synthesized Bi_2S_3 nanorods prepared by a sonochemical method from an aqueous solution of bismuth nitrate and sodium thiosulfate in the presence of complexing agents.

To the best of our knowledge, few articles have simultaneously presented an introduction of Bi_2S_3 into TiO_2 by a sonochemical synthesis route and discussed their different effects on the visible-light-driven photocatalytic efficiency of industrial dyes. In this work, we report a simple and green route for the preparation of Bi_2S_3-TiO_2 heterostructured nanocomposites through an ultrasonic treatment under room-temperature conditions. The evolution of reactive oxygen species was also investigated by the oxidation of 1,5-diphenylcarbazide (DPCI) into 1,5-diphenylcarbazone (DPCO), which can be extracted by organic solvents and which clearly displays absorbance in a certain range of wavelength.[16]

2. Experimental Procedure

2.1. Materials

Ethylene glycol, ammonium hydroxide (NH_4OH, 28%) and anhydrous ethanol were purchased from Daejung Chemical Co. (Korea). Titanium oxide nanopowder (TiO_2, < 25 nm, 99.7%) with the anatase structure used as an original sample was purchased from Sigma-Aldrich Chemistry, USA. Bismuth nitrate ($Bi(NO_3)_3 \cdot 5H_2O$) and sodium sulfide·5-hydrate ($Na_2S \cdot 5H_2O$) were used for the preparation of Bi_2S_3 and were supplied by Duksan Pure Chemical Co., Ltd, Korea and by Yakuri Pure Chemicals Co., Ltd, Japan, respectively. 1,5-diphenylcarbazide (DPCI) and Texbrite BA-L (TBA) were purchased from Daejung Chemicals & Metals and from Texchem Korea Co. Ltd., Korea, respectively. All chemicals were used without further purification and all experiments were carried out using distilled water.

2.2. Synthesis of Bi_2S_3/TiO_2 nanocomposites

TiO_2 nanoparticles were prepared according to a previous method by the authors.[17] The detailed process is as follows: first, TiO_2 precursors were prepared with a molar ratio of ethanol: H_2O: TNB of 35 : 15:4, and the suspension was sonicated at room temperature for 2 h. The final products were filtered and washed repeatedly and then dried under a vacuum at 373 K. The dried catalyst was ground in a ball mill and calcined at 773 K for 1 h to obtain TiO_2 nanoparticles. Fig. 1 shows an image of the synthesis process of the Bi_2S_3/TiO_2 nanocomposites. Initially, 0.4 g of TiO_2 powder was added to 70 mL of ethyl alcohol containing 5 mL NH_4OH, which introduces more hydroxyl groups adsorbed onto the surface of TiO_2.[18] The defined amount of $Bi(NO_3)_3 \cdot 5H_2O$ was dissolved in the above solution, which was then vigorous stirred and sonicated (at 750 W, Ultrasonic Processor VCX 750, Korea)) for 30 min at a temperature of 353 K. Afterward, the $Na_2S \cdot 5H_2O$ solution (30mL) was dropwise added to the solution, followed by ultrasonication for another 3 h. Subsequently, the temperature of the mixture was reduced to room temperature and the mixture was filtered using Whatman filter paper and washed with distilled water and ethanol five times. The dried catalyst was labeled Bi_2S_3/TiO_2. For comparison, a pure Bi_2S_3 photocatalyst was synthesized using a similar procedure.

2.3. Instrumentation

To determine the crystal phase and the composition of the as-prepared pure TiO_2, Bi_2S_3, and Bi_2S_3/TiO_2 samples, XRD characterizations were carried out at room temperature using an XRD device (Shimata XD-D1, Japan) with Cu Kα radiation (l=1.54056 Å) in the range of $2\theta = 10 - 80^{\circ}$ at a scan speed of $1.2^{\circ}\,m^{-1}$. A SEM instrument (JSM-5200 JOEL, Japan) was used to observe the surface state and morphology of the prepared nanocomposites. Energy dispersive X-ray spectroscopy (EDX) was employed for an elemental analysis. Transmission electron microscopy (TEM, JEOL, JEM-2010, Japan) was used to observe the surface state and structure of the photocatalyst composites at an acceleration voltage of 200 kV. The decomposition kinetics for the photocatalytic activity was measured using a spectrometer (Optizen POP, MECASYS, Korea).

2.4. Evaluation of Reactive Oxygen Species

First, four 100 mL transparent volumetric flasks were

marked a through d. Four 10.00 mL DPCI stock solutions (1.00×10^{-2} mol/L) were added to each of these flasks, followed by the addition of 50 mg of the Bi_2S_3/TiO_2 sample in the order of (1, 2, 3, 4) from a to d. All four solutions were diluted to 100 mL with double-distilled water. The final DPCI concentration and Bi_2S_3/TiO_2 amount were 1.00×10^{-3} mol/L and 1.00 g/L, respectively. First, the experiment was performed without sample powder under the same condition and the DPCL solution was illuminated in a visible light condition. After 120 min of irradiation, 10 ml of the solution was removed from each reactor with an extraction step following with benzene. In the second step, all of the extracted solutions were diluted to 10 mL with the benzene solution and their UV-Vis spectra were recorded using a spectrometer.

2.5. Photocatalytic Performance

The photocatalytic performances of the pure TiO_2, P25, the as-prepared Bi_2S_3, and the Bi_2S_3/TiO_2 were evaluated using the degradation of Texbrite BA-L (TBA) as an industrial dye under visible light radiation. A 24 W visible light source served as the simulated light source. In each run, 10 mg of the photocatalysts were placed in a 60 ml solution of Texbrite BA-L (TBA) (0.1 mg ml^{-1}). Before irradiation, the solution remained in the dark to establish adsorption/desorption equilibrium. The visible light was then switched on. At given time intervals, the collected samples were centrifuged for 10 minutes to remove the solid materials instantly for further analysis. The photocatalytic behavior of the samples was analyzed through the absorbance spectrometry with a UV/Vis spectrophotometer (Optizen POP, MECASYS, Korea).

3. Results and Discussion

3.1. Structural analysis

X-ray diffraction patterns of all pure TiO_2, the P25, the as-prepared Bi_2S_3, and the Bi_2S_3/TiO_2 are shown in Fig. 2, in which several reflections corresponding to characteristic interplanar spacing can be observed. It can be confirmed that the TiO_2 in the as-prepared photocatalysts is in the anatase phase, while the Ag_2Se appears to be the predominant crystalline phase of acanthite. For these three samples, the (101), (004), (211), and (204) crystal planes originated from the anatase TiO_2 phase with the orthorhombic phase showing good crystallinity, which is consistent with the data reported for Bi_2S_3 (JCPDS Card File No. 17-0320).[19] After being introduced into TiO_2, it can clearly be seen that the intensity of the Bi_2S_3 peaks decreased, confirming the synthesis of homogeneously dispersed Bi_2S_3 and TiO_2 nanocrystals. The particles size D of Bi_2S_3 was calculated using the Scherrer formula,

$$D = K\lambda / \beta \cos Q_B \quad (1)$$

where β is the full width at half maxima, K is a shape factor

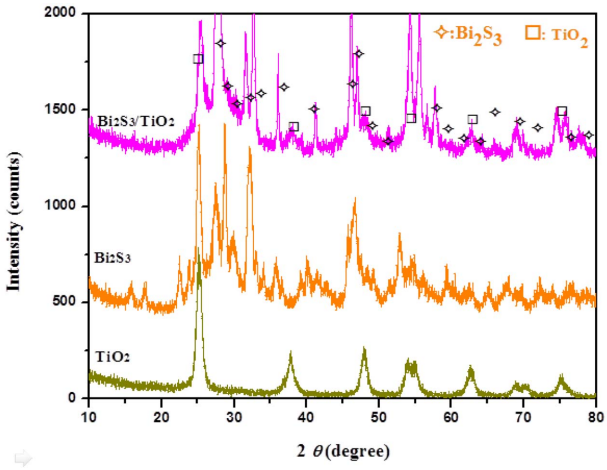

Fig. 2. XRD patterns of as-prepared samples: TiO_2, Bi_2S_3 and Bi_2S_3/TiO_2 nanocomposites.

(= 0.9), and l is the wavelength of the incident X-ray. The average particle size falls in the range of 25 nm, indicating the nano size of the Bi_2S_3 particles.

3.2. Surface characteristics of the samples

The micro-surface structures and morphologies of the as-prepared Bi_2S_3 and Bi_2S_3/TiO_2 were characterized by SEM (Fig. 3(a)). The SEM technique is used to inspect the topographies of specimens at very high magnification levels using equipment known as a scanning electron microscope. Fig. 3 shows the macroscopic changes in the morphology of the composites. In Fig. 3(a), Bi_2S_3 shows a small particle size and a good dispersion. Zhang *et al.* reported that a good dispersion of small particles can provide more reactive sites for reactants as compared to aggregated particles.[20] Comparing with the Bi_2S_3 and Bi_2S_3/TiO_2 samples (Figs. 3(a) and (b)), the Bi_2S_3 particles were fixed onto the TiO_2 surface and the

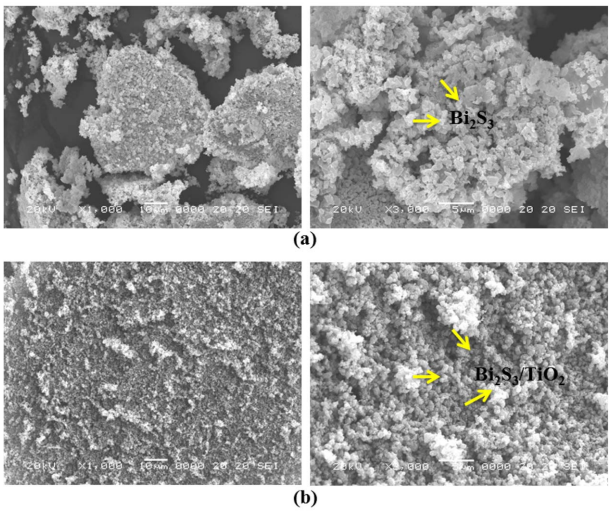

Fig. 3. SEM micrographs of as-prepared samples: (a) Bi_2S_3 and (b) Bi_2S_3/TiO_2 nanocomposites.

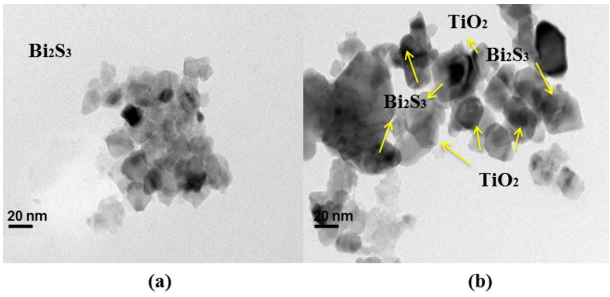

Fig. 4. TEM micrographs of as-prepared samples: (a) Bi_2S_3 and (b) Bi_2S_3/TiO_2 nanocomposites.

distribution was uniform, but the particles were more numerous and larger than those of pure Bi_2S_3 with a slight tendency to agglomerate. This type of agglomeration can occur when the crystal particle size is very small due to the weak surface forces of TiO_2.[21)]

The microscopic structural information of the as-prepared Bi_2S_3 and Bi_2S_3/TiO_2 composites is shown in Figs. 4(a) and (b). The TEM images revealed that the Bi_2S_3/TiO_2 sample displayed well-dispersed Bi_2S_3 nanoparticles with an average size of around 15 - 25 nm, as particle agglomeration was effectively inhibited during the introduction of the anatase TiO_2 nanoparticles. The nanoscale TiO_2 displayed well-dispersed nanoparticles with an average size of 20 nm, as clearly shown in Fig. 4(b). The presence of a distinct juncture between the two crystal phases confirmed the strong interaction between Bi_2S_3 and TiO_2 in Bi_2S_3/TiO_2, further indicating the heterogeneous structure. This indicates that the ultrasonic-assisted synthesis of Bi_2S_3/TiO_2 is advantageous over other synthesis methods and would improve the photocatalytic properties of these materials.[22)]

3.3. Elemental analysis of the preparation

A chemical composition analysis was conducted and the element weight percentage values of the prepared Bi_2S_3 and Bi_2S_3/TiO_2 composites were examined by EDX. Fig. 5 shows the element weight percentages of prepared Bi_2S_3 and Bi_2S_3/TiO_2 composites. It shows that strong Kα and Kβ peaks from Ti element appear at 4.51 and 4.92 keV, while a moderate Kα peak of the element O appears at 0.52 keV.[23)] It was found that the strong Kα peak from the S element appears at 2.37 keV, while a Lα peak from Bi element appears at 10.84 keV.[24,25)] Fig. 5(c) shows the presence of O, Ti, Bi and S as major elements with strong peaks; thus, a highly pure Bi_2S_3/TiO_2 nanocomposite was successfully synthesized.

3.4. Generation of ROS

Figure 6 shows the UV–Vis spectra of DPCO extract liquors in the presence of Bi_2S_3/TiO_2 nanocomposites as well as a test without samples. The four reaction solutions, as discussed earlier, were placed in an ultrasonic chamber in a 200 ml borosilicate glass container. Under ultrasonic irradiation, 1,5-diphenylcarbazide (DPCI) can be oxidized by oxidizing substances into 1,5-diphenylcarbazone (DPCO). Under visible light, Bi_2S_3/TiO_2 nanocomposites are excited to a higher energy state. That is, some electrons are transmitted from the valence band (VB) to the conduction band (CB). Meanwhile, the generated electron hole pair is formed by the Bi_2S_3. Simultaneously, the excited electron is transferred from the conduction band of Bi_2S_3 to the TiO_2 surface. The obtained ·OH radicals can oxidize 1,5-diphenylcarbazide (DPCI) into 1,5-diphenylcarbazone (DPCO). The DPCO was extracted by the benzene solvent. The absorbance spectra of our nanocomposites and the observed absorbance peaks around 400 nm are in agreement with the results reported in the literature.[26,27)]

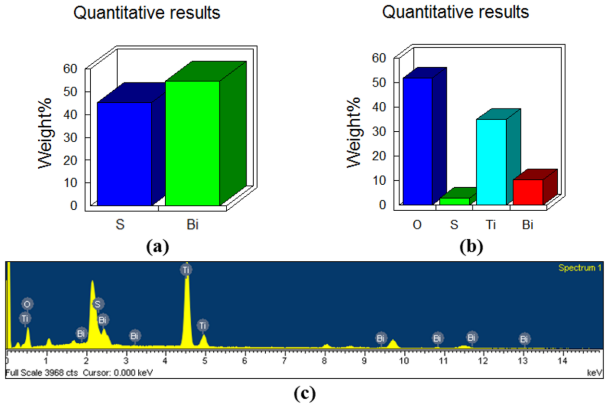

Fig. 5. Element weight percentage (a), (b) and EDX elemental microanalysis results (c) of the as-prepared samples: Bi_2S_3 and Bi_2S_3/TiO_2 nanocomposites.

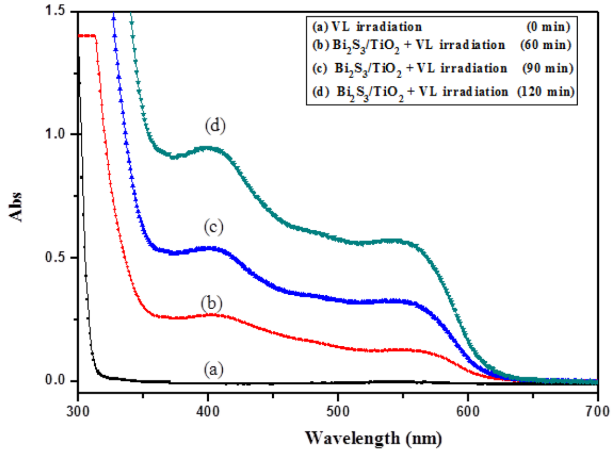

Fig. 6. UV-Vis spectra of the DPCO extract liquors (a), and of the liquors in the presence of the Bi_2S_3/TiO_2 nanocomposite photocatalyst under visible-light irradiation for 60 mins (b), 90 mins (c) and 120 mins (d).

3.5. Adsorption properties

To evaluate the adsorption ability of the as-prepared composite catalysts, the reactor was placed on the magnetic churn dasher while stirring it for 120 min in a dark box to establish a state of adsorption–desorption equilibrium.

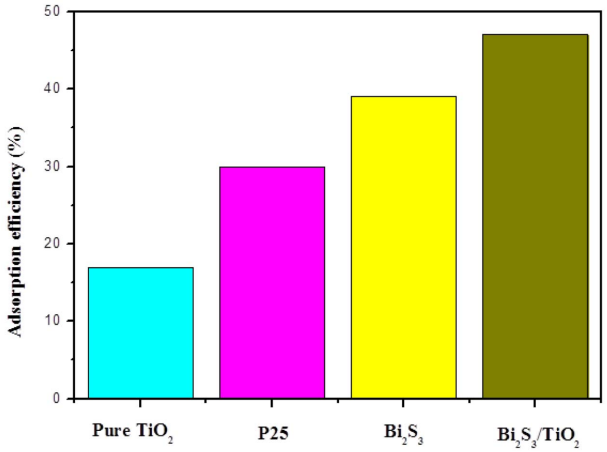

Fig. 7. Adsorption effect of the Texbrite BA-L (TBA) concentration after adsorption–desorption equilibrium.

From the result shown in Fig. 7, the level of TBA adsorption by Bi_2S_3/TiO_2 was higher than that of the TiO_2, P25 and Bi_2S_3 control samples. This can be attributed to the large surface area of the Bi_2S_3/TiO_2 catalysts of approximately 42.58 m^2/g, which is likely correlated with the strong adsorption ability. The surface area of Bi_2S_3 is about 36.71 m^2/g, which is higher than that of the pure TiO_2 sample of about 18.64 m^2/g. The surface area of P25 was similar to that of the TiO_2 catalysts at about 19.95 m^2/g. After establishing adsorption–desorption equilibrium for the Bi_2S_3/TiO_2 catalyst, the TBA dye solution was removed at a rate of approximately 47% while the TBA solution was removed at only 17% for pure TiO_2.

3.6. Degradation effects of Texbrite BA-L (TBA)

The photocatalytic activity of the as-prepared nanocomposite was evaluated by the catalytic degradation of Texbrite BA-L (TBA) as an industrial dye under visible-light irradiation. As shown in Fig. 8(a), the absorbance of anatase TiO_2 is lower than that of the Bi_2S_3/TiO_2 composites because pure TiO_2 cannot be actively excited by visible-light irradiation. Similar results were also observed by Yu *et al.*[28] The photocatalytic degradation of the TBA solution with the Bi_2S_3/TiO_2 composite was better than any of the other composites. These results can be mainly explained as follows: small particles which are well dispersed can provide more reactive sites for reactants than aggregated particles.[29] As noted above with regard to the surface characteristics, the Bi_2S_3/TiO_2 composite has a favorable morphology for the adsorption of relatively more organic pollutants. In addition, the favorable morphology also played an important role in shuttling visible light photo-induced electrons generated from Bi_2S_3 into the conduction band of TiO_2 efficiently.

The photocatalytic degradation effect for different photocatalysts under visible light obeys the pseudo-first-order kinetics with respect to the concentration of TBA:

$$-dc/dt = k_{app}c$$

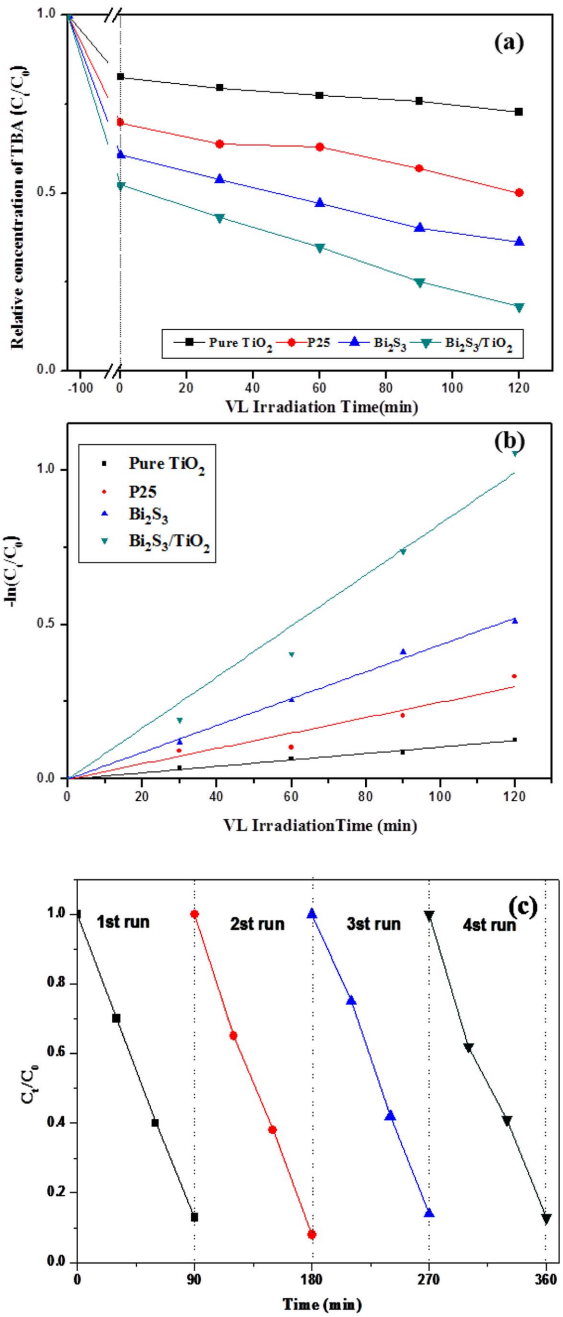

Fig. 8. (a) Relative concentration of Texbrite BA-L (TBA) adsorption and degradation, (b) apparent first-order kinetics of Texbrite BA-L (TBA) visible-light photocatalysis degradation against TiO_2, P25, Bi_2S_3 and Bi_2S_3/TiO_2, and (c) cycling runs regarding the degradation of Texbrite BA-L (TBA) with Bi_2S_3/TiO_2 under visible-light irradiation.

Integrating this equation (with the restriction of $c = c_0$ at $t = 0$, with c_0 being the initial concentration in the bulk solution after dark adsorption and t being the reaction time) will lead to the following expected relationship,

$$-\ln(c_t/c_0) = k_{app}t,$$

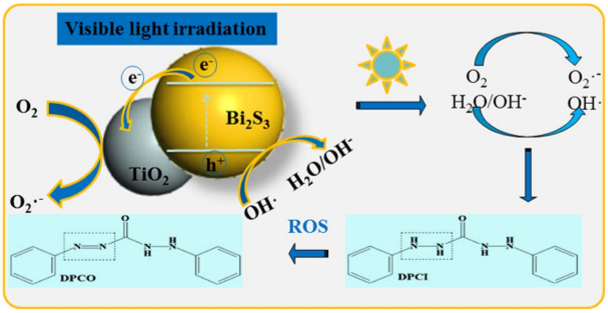

Fig. 9. The scheme of the degradation of Texbrite BA-L (TBA) and ROS generation at the Bi_2S_3/TiO_2 interface under visible-light irradiation.

where c_t and c_0 are the reactant concentrations at times $t = t$ and $t = 0$, respectively, and k_{app} and t are correspondingly the apparent reaction rate constant and time. According to this equation, a plot of $-\ln(c_t/c_0)$ versus t will yield a slope of k_{app}. According to the results displayed in Fig. 8(b), (c), the Texbrite BA-L (TBA) degradation rate constant for Bi_2S_3/TiO_2 composites reaches 8.27×10^{-3} min^{-1} under visible light, much higher than the corresponding values for pure Bi_2S_3 (4.34×10^{-3} min^{-1}), P25 (2.49×10^{-3} min^{-1}), and the value of 1.04×10^{-3} min^{-1} for TiO_2. These results further confirm that the Bi_2S_3/TiO_2 nanocomposite is a much more effective catalyst material than the other samples.

To demonstrate the stable cyclic performance of the Bi_2S_3/TiO_2 photocatalyst, consecutive photocatalytic Texbrite BA-L (TBA) degradation reactions were conducted under visible-light irradiation. As shown in Fig. 8(c), Bi_2S_3/TiO_2 did not exhibit any significant loss of photocatalytic activity after four runs of Texbrite BA-L (TBA) degradation. These results indicate that the Bi_2S_3/TiO_2 photocatalyst is highly stable and is not photo-corroded during the photocatalytic oxidation of Texbrite BA-L (TBA). TiO_2 modification with a semiconductor not only improves the photocatalytic performance but also realizes the long-term stability of Bi_2S_3 nanocrystals.[15] This result is significant from a practical viewpoint, as the enhanced photocatalytic activity and stability will lead to more cost-effective operation. These results further confirm that Bi_2S_3/TiO_2 can be used as a catalytic material in environmental purification processes or in waste-water treatment facilities in the future.

In our nanosized Bi_2S_3 coupled TiO_2 nanocomposite system, the coupling of two such semiconductors plays a beneficial role in improving charge separation and extending the use of TiO_2 in response to visible light. Based on the literature,[30,31] we propose a mechanism for the degradation of pollutants and the generation of ROS under visible-light irradiation, as shown in Fig. 9. Visible-light irradiation produces electrons (e^-) in the conduction band (CB) and holes (h^+) in the valence band (VB) of Bi_2S_3 in the nanocomposite. Meanwhile, the generated electron is transferred to the CB of Bi_2S_3, thereby increasing the number of electrons as well as the rate of electron-induced redox reactions. Graphene coupled with the Bi_2S_3-supported system shows enhanced catalytic activity due to the high charge separation induced by the synergetic effects of TiO_2 and Bi_2S_3. The generated electrons (e^-) react with the dissolved oxygen molecules and produce oxygen peroxide radicals, $O_2^{\bullet-}$. The positive charge hole (h^+) can react with OH^- derived from H_2O to form hydroxyl radicals, $OH^\bullet$. The Texbrite BA-L (TBA) may be degraded by the $O_2^{\bullet-}$ oxygen peroxide radicals and the $OH^\bullet$ hydroxyl radicals to CO_2, H_2O, or other mineralization products.[32]

4. Conclusions

In conclusion, we synthesized Bi_2S_3/TiO_2 nanocomposites through simple ultrasonic-assisted techniques. XRD result shows that titanium dioxide is in the anatase phase. The orthorhombic phase of Bi_2S_3 can be observed clearly, and the introduction of TiO_2 prevents the growth of crystal Bi_2S_3. TEM microphotographs show that the TiO_2 particles are homogenously coated by the Bi_2S_3 particles uniformly, indicating that particle agglomeration is effectively inhibited after the introduction of anatase TiO_2 nanoparticles. The high catalytic efficiency is attributed to the loading of Bi_2S_3 particles, which is helpful to separate the generated carriers effectively and to improve the surface properties of the catalysts. The quantities of generated hydroxyl radicals can be analyzed by DPCI degradation, and it was proved here that under visible-light irradiation, more electron–hole pairs can be generated. It is expected that this work will offer valuable references with regard to the study of the reaction mechanism of visible-light photocatalytic degradation to promote its applications to environmental treatments and new methods of the use of energy.

REFERENCES

1. A. Z. Abdullah and P. Y. Ling, "Heat Treatment Effects on the Characteristics and Sonocatalytic Performance of TiO_2 in the Degradation of Organic Dyes in Aqueous Solution," *J. Hazard. Mater.*, **173** [1-3] 159-67 (2010).
2. M. Inoue, F. Okada, A. Sakurai, and M. Sakakibara, "A New Development of Dyestuffs Degradation System Using Ultrasound," *Ultrason. Sonochem.*, **13** [4] 313-20 (2006).
3. L. Zhu and W. C. Oh, "Review for Semiconductor/Reduced Graphene Oxide Nanocomposites: Fabrication, Characterization and Application for Decontamination of Organic Dyes," *J. Multifunct. Mater. Photosci.*, **5** [2] 153-70 (2014).
4. K. Hashimoto, H. Irie, and A. Fujishima, "TiO_2 Photocatalysis: a Historical Overview and Future Prospects," *Jpn. J. Appl. Phys.*, **44** [12] 8269-85 (2005).
5. A. L. Linsebigler, G. Q. Lu, and J. T. Yates, "Photocatalysis on TiO_2 Surfaces: Principles, Mechanisms, and Selected Results," *Chem. Rev.*, **95** [3] 735-58 (1995).
6. W. H. Dong, F. Pan, L. L. Xu, M. R. Zheng, C. H. Sow, K. Wu, G. Q. Xu, W. Chen, "Facile Synthesis of CdS@TiO_2 Core-Shell Nanorods with Controllable Shell Thickness and Enhanced Photocatalytic Activity under Visible Light

Irradiation," *Appl. Sur. Sci.*, **349** 279-86 (2015).
7. X. L. Zhang, Y. H. Tang, Y. Li, Y. Wang, X. N. Liu, C. B. Liu, and S. L. Luo, "Reduced Graphene Oxide and PbS Nanoparticles Co-Modified TiO_2 Nanotube Arrays as a Recyclable and Stable Photocatalyst for Efficient Degradation of Pentachlorophenol," *Appl. Catal. A: Gen.*, **457** 78-84 (2013).
8. Q. Shen, D. Arae, and T. Toyoda, "Photosensitization of Nanostructured TiO_2 with CdSe Quantum Dots: Effects of Microstructure and Electron Transport in TiO_2 Substrates," *J. Photochem. Photobiol. A,* **164** [1-3] 75-80 (2004).
9. I. Robel, V. Subramanian, M. Kuno, and P. V. Kamat, "Quantum Dot Solar Cells. Harvesting Light Energy with CdSe Nanocrystals Molecularly Linked to Mesoscopic TiO_2 Films," *J. Am. Chem. Soc.*, **128** [7] 2385-93 (2006).
10. O. Rabin, J. M. Perez, J. Grimm, G. Wojtkiewicz, and R. Weissleder, "An X-ray Computed Tomography Imaging Agent Based on Long-Circulating Bismuth Sulphide Nanoparticles," *Nat. Mater.*, **5** 118-22 (2006).
11. H. Yu, J. Huang, H. Zhang, Q. Zhao, and X. Zhong, "Nanostructure and Charge Transfer in Bi_2S_3-TiO_2 Heterostructures," *Nanotechnology*, **25** [21] 215702 (2014).
12. Y. Bessekhouad, D. Robert, and J. V. Weber, "Bi_2S_3/TiO_2 and CdS/TiO_2 Heterojunctions as an Available Configuration for Photocatalytic Degradation of Organic Pollutant," *J. Photochem. Photobio. A*, **163** [3] 569-80 (2004).
13. M. Salavati-Niasari, G. Hosseinzadeh, and F. Davar, "Synthesis of Lanthanum Carbonate Nanoparticles via Sonochemical Method for Preparation of Lanthanum Hydroxide and Lanthanum Oxide Nanoparticles," *J. Alloy Compd.*, **509** [1] 134-40 (2011).
14. M. Esmaeili-Zare, M. Salavati-Niasari, and A. Sobhani, "Simple Sonochemical Synthesis and Characterization of HgSe Nanoparticles," *Ultrason. Sonochem.*, **19** [5] 1079-86 (2012).
15. H. Wang, J. J. Zhu, J. M. Zhu, and H. Y. Chen, "Sonochemical Method for the Preparation of Bismuth Sulfide Nanorods," *J. Phys. Chem. B*, **106** [15] 3848-54 (2002).
16. J. Wang, Y. W. Guo, B. Liu, X. D. Jin, L. J. Liu, R. Xu, Y. M. Kong, and B. X. Wang, "Detection and Analysis of Reactive Oxygen Species (ROS) Generated by Nano-Sized TiO_2 Powder under Ultrasonic Irradiation and Application in Sonocatalytic Degradation of Organic Dyes," *Ultrason. Sonochem.*, **18** [1] 177-83 (2011).
17. L. Zhu, G. Trisha, C. Y. Park, Z. D. Meng, and W. C. Oh, "Enhanced Sonocatalytic Degradation of Rhodamine B by Graphene-TiO_2 Composites Synthesized by an Ultrasonic-Assisted Method," *Chin. J. Catal.*, **33** [7-8] 1276-83 (2012).
18. M. E. Simonsen, Z. S. Li, and E. G. Søgaard, "Influence of the OH Groups on the Photocatalytic Activity and Photoinduced Hydrophilicity of Microwave Assisted Sol–Gel TiO_2 Film," *Appl. Surf. Sci.*, **255** 8054-62 (2009).
19. Y. Y. Zhao, K. Ting, E. Chua, C. K. Gan, J. Zhang, B. Peng, Z. P. Peng, and Q. H. Xiong, "Phonons in Bi_2S_3 Nanostructures: Raman Scattering and First-Principles Studies," *Phys. Rev. B*, **84** [20] 205330 (2011).
20. X. W. Zhang, M. H. Zhou, and L. C. Lei, "Preparation of Photocatalytic TiO_2 Coatings of Nanosized Particles on Activated Carbon by AP-MOCVD," *Carbon*, **43** [8] 1700-8 (2005).
21. D. W. Kim, D. S. Kim, Y. G Kim, Y. C. Kim, and S. G. Oh, "Preparation of Hard Agglomerates Free and Weakly Agglomerated Antimony Doped Tin Oxide (ATO) Nanoparticles by Coprecipitation Reaction in Methanol Reaction Medium," *Mater. Chem. Phys.*, **97** 452-57 (2006).
22. K. K. Akurati, A. Vital, J. P. Dellemann, K. M. Michalow, D. Ferri, T. Graule, and A. Baiker, "Flame-Made WO_3/TiO_2 Nanoparticles: Relation between Surface Acidity, Structure and Photocatalytic Activity," *Appl. Catal. B: Environ.*, **79** [1] 53-62 (2008).
23. L. Zhu, S. B. Jo, S. Ye, K. Ullah, Z. D. Meng, and W. C. Oh, "A Green and Direct Synthesis of Photosensitized CoS_2–Graphene/TiO_2 Hybrid with High Photocatalytic Performance," *J. Ind. Eng. Chem.*, **22** 264-71 (2015).
24. L. Zhu, Z. D. Meng, and W. C. Oh, "MWCNT-Based Ag_2S-TiO_2 Nanocomposites Photocatalyst: Ultrasound-Assisted Synthesis, Characterization, and Enhanced Catalytic Efficiency," *J. Nanomater.*, **2012** 1-10 (2012).
25. P. Pusit, K. Suchanya, P. Ratchadaporn, S. Supaporn, and P. Sukon, "Preparation and Characterization of $BiVO_4$ Powder by the Sol–Gel Method," *Ferroelectrics.*, **456** 45-54 (2013).
26. K. John, D. T. Manolis, D. P. George, N. A. Mariza, S. T. Kostas, G. Sofia, B. Kyriakos, K. Christos, O. Michael, and L. Alexis, "Highly Active Catalysts for the Photooxidation of Organic Compounds by Deposition of [60] Fullerene onto the MCM-41 Surface: A Green Approach for the Synthesis of Fine Chemicals," *Appl. Catal., B,* **117-118** 36-48 (2012).
27. Z. D. Meng, L. Zhu, K. Ullah, S. Ye, and W.C. Oh, "Detection of Oxygen Species Generated by WO_3 Modification Fullerene/TiO_2 in the Degradation of 1,5-diphenyl Carbazide," *Mater. Res. Bull.*, **56** 45-53 (2014).
28. X. D. Yu, Q. Y. Wu, S. C. Jiang, and Y. H. Guo, "Nanoscale ZnS/TiO_2 Composites: Preparation, Characterization, and Visible-Light Photocatalytic Activity," *Mater. Charact.*, **57** [4-5] 333-41 (2006).
29. F. J. Zhang, J. Liu, M. L. Chen, and W. C. Oh, "Photo-Electrocatalytic Degradation of Dyes in Aqueous Solution Using CNT/TiO_2 Electrode," *J. Korean Ceram. Soc.*, **46** [3] 263-70 (2009).
30. H. Li, B. Zhu, Y. Feng, S. Wang, S. Zhang, and W. Huang, "Synthesis, Characterization of TiO_2 Nanotubes-Supported MS (TiO_2NTs@MS, M=Cd, Zn) and their Photocatalytic Activity," *J. Solid. State. Chem.*, **180** [7] 2136-42 (2007).
31. Y. Xie, S. H. Heo, Y. N. Kim, S. H. Yoo, and S. O. Cho, "Improved Conversion Efficiency of CdS Quantum Dots-Sensitized TiO_2 Nanotube Array Using ZnO Energy Barrier Layer," *Nanotechnology*, **22** [1] 015702 (2010).
32. O. K. Dalrymple, E. Stefanakos, M. A. Trotz, and D. Y. Goswami, "A Review of the Mechanisms and Modeling of Photocatalytic Disinfection," *Appl. Catal. B: Environ.*, **98** [1-2] 27-38 (2010).